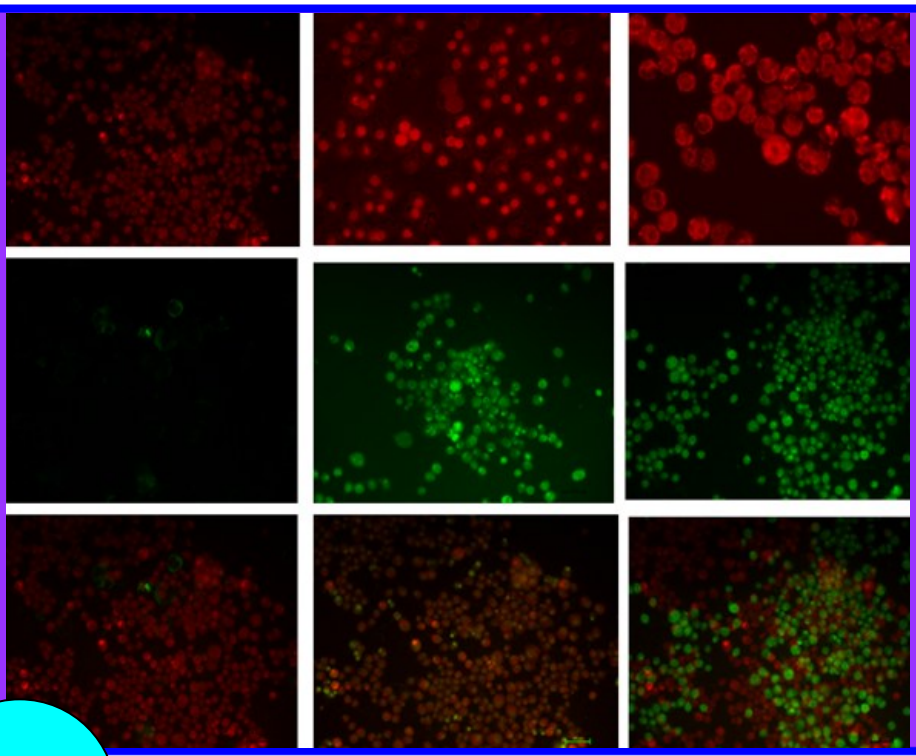

BJP

Bangladesh Journal of Pharmacology

Research Article

Novel CRT2 peptide inhibits tumor growth and angiogenesis in colorectal cancer HT-116 cell lines via PI3K/ERK signaling pathway

A Journal of the Bangladesh Pharmacological Society (BDPS)
Journal homepage: www.bdpsjournal.org; www.banglajol.info
Abstracted/indexed in Academic Search Complete, Agroforestry Abstracts, Asia Journals Online, Bangladesh Journals Online, Biological Abstracts, BIOSIS Previews, CAB Abstracts, Current Abstracts, Directory of Open Access Journals, EMBASE/Excerpta Medica, Global Health, Google Scholar, HINARI (WHO), International Pharmaceutical Abstracts, Open J-gate, Science Citation Index Expanded, SCOPUS and Social Sciences Citation Index
Bangladesh J Pharmacol 2025; 20: 89-100
ISSN: 1991-0088

Novel CRT2 peptide inhibits tumor growth and angiogenesis in colorectal cancer HT-116 cell lines via PI3K/ERK signaling pathway

Dhanapal Yogananthan[1], Ashok Raj Kattur Venkatachalam[2], and Ramanathan Muthiah[1]

[1]Department of Pharmacology, PSG College of Pharmacy, Coimbatore, Tamil Nadu-641004, India; [2]Department of Microbiology, PSG College of Arts and Science, Coimbatore, Tamil Nadu-641014, India.

Article Info

Received: 10 May 2025
Accepted: 11 July 2025
Available Online: 31 August 2025
DOI: 10.3329/bjp.v20i3.81605

Cite this article:
Yogananthan D, Venkatachalam ARK, Muthiah R. Novel CRT2 peptide inhibits tumor growth and angiogenesis in colorectal cancer HT-116 cell lines via PI3K/ERK signaling pathway. Bangladesh J Pharmacol. 2025; 20: 89-100.

Abstract

This study aims to evaluate the efficacy of the CRT2 peptide in inhibiting VEGFR1 tyrosine kinase activity against solid tumors. Molecular docking was performed using Cluspro 2.0 against the vascular endothelial growth factor receptor-1 (VEGFR1) with CRT2. Moreover, *in vitro* studies were conducted using colorectal cancer HT-116 cell lines to investigate apoptosis, cell cycle analysis, and peptide binding assays. The MTT assay revealed a significant variation in the IC_{50} value, with a result of 16.0 µg/mL. The anti-cancer activity of CRT2 was by apoptosis (45.7%) and dose-dependent cell cycle G1/S phase arrest in colorectal cancer cell lines. Furthermore, the consequences showed that CRT2 deterred the PI3K/Akt signaling pathway in a dose-dependent manner. The outcomes of the present study indicate that CRT2 employed selective anti-cancer effects on HT-116 cell lines through cell cycle arrest, apoptosis, and inhibition of the PI3K/Akt signaling pathways.

Introduction

Colorectal cancer is characterized by genetic abnormalities that lead to uncontrolled cell proliferation in the colorectal region (Baidoun, 2021; Weitz et al., 2005). Conventional cancer therapies, such as chemotherapy, often have significant adverse effects. Consequently, when these drugs are administered systemically, tumor cells can develop resistance due to alterations in metabolism, gene mutation, and epigenetic modifications. Highly metastatic cells are typically mutant cells. Metastasis results from the balance between pro- and anti-angiogenic growth factors, which, when present in high concentrations, can promote the growth of tumor cells.

Vascular endothelial growth factor (VEGF) provides essential nutrients to tumor cells. Angiogenesis and tumor metastasis are significantly influenced by the release of pro-angiogenic factors from both endothelial and tumor cells (Mabeta et al., 2022). The VEGF family exerts its biological effects through interactions with the transmembrane tyrosine kinases, including vascular endothelial growth factor receptor (VEGFR1 or VEGFR2). Through signal transduction molecules PI3K and ERK1/2, the high-affinity ligands for VEGFR1, including VEGF-A, VEGF-B, PIGF, and VEGF-C, bind to VEGF-A, VEGF-C, and VEGF-E, activating the downstream signaling pathways involving PI3K and ERK1/2. This ligand-receptor interaction triggers signaling pathways that promote cell invasion, migration, proliferation, and enhanced vascular permeability (Wang, 2020; Zanjanchi et al., 2022). Most studies have focused on the VEGF/VEGFR anti-angiogenic signaling pathways involved in the VEGF and VEGFR. However, monoclonal antibody treatments face several therapeutic challenges, including suboptimal pharmacokinetics, significant therapeutic resistance, and diminished sensi-

tivity in clinical outcomes. These therapies target anti-VEGF and small-molecule inhibitors of tyrosine kinases. Additionally, peptides have emerged as a promising new class of therapeutics.

Numerous bioactive peptide compounds consisting of modest molecular weight fragments, typically ranging from 10 to 20 amino acid residues, have recently been the focus of research as potentially active pharmacological agents to enhance health (Dia et al., 2016). In contrast, BG-4, a newly discovered peptide derived from bitter groundnuts, demonstrates anti-cancer activity against HT-29, HT-116, and SW420 cancer cell lines (Shanthosa et al., 2013).

Garlic (*Allium sativum*) is a well-known plant recognized for its nutriational and preventive health benefits. Garlic contains organosulfur compounds, such as diallyl derivatives, which have demonstrated anti-cancer effects across various tumor models in both *in vitro* and *in vivo* systems (He et al., 2013). Among these, the garlic-derived peptide VS-9 has significant anti-leukemic activity against K562 and MOLT-4 cell lines through its interaction with the Bid-BH3 complex proteins, which are key regulators in apoptotic pathways. Programmed cell death (apoptosis) is a cell-controlled biological process that can be triggered via extrinsic or intrinsic stimuli (Dey, 2021; Zhang et al., 2021). Central to the intrinsic pathway are the Bcl-2 family proteins, which function as critical regulators of cell survival and mitochondrial-mediated apoptosis. Recent investigations have further expanded the scope of targeted therapies by focusing on the Bcl-2 protein family, which also acts as a proto-oncogene and an integral membrane protein involved in tumor progression.

Based on both *in vitro* and *in vivo* findings, novel peptides targeting vascular endothelial growth factor receptors, such as VGB4, have been developed to specifically inhibit VEGFR1 and VEGFR2 signaling pathways (Behelgardi et al., 2013). Notably, the VGBE peptide demonstrated potent anti-angiogenic properties by impairing human umbilical vein endothelial cell (HUVEC) colony formation, invasion, migration, and differentiation. The overarching aim of these approaches is to develop targeted anti-VEGFR1 peptides with therapeutic potential for the cancer.

Materials and Methods

Chemicals

Penicillin-streptomycin (15140163), DPBS (10010023), A4766801), DMEM high glucose (11965118), were purchased from Thermo Scientific, USA, and the annexin V-FITC Kit (IM3546) from Beckman Coulter Life Science, USA. The antibodies cytochrome C (ab133504), anti-Bax (ab182733), anti-Bcl-2 (ab32124), anti-β-actin antibody-loading control (ab8226), anti-p21, anti-cyclin-D1 (ab26), anti-PI3K, anti-ERK1/2, and anti-jnk1/2 (Abeam Cambridge, UK) were purchased.

National Centre for Cell Science, Pune, India, provided colorectal cancer cell lines.

CRT2 peptide synthesis

The CRT2 peptide (VKLRSLLCSRMMRMMRRM-OH) was synthesized using Fmoc-based solid-phase peptide synthesis on Rink amide resin. Standard coupling protocols were followed (Yoganantham et al. 2023). After assembly, the peptide was cleaved from the resin using a trifluoroacetic acid cleavage mixture and precipitated with cold diethyl ether. The crude peptide was then purified using ultra-performance liquid chromatography with a Waters Nano Quality Empower-2.0 system. The final product exhibited a purity of 95%, and its molecular weight was confirmed using LC-MS/MS analysis.

In silico structural biology

The 3D structure of the CRT2 peptide was predicted using the PEP-FOLD3 server. Ligand conformations were generated and optimized using the LigPrep module of Schrödinger. The crystal structure of VEGFR1 (PDB ID: 2XAC) was retrieved from the Protein Data Bank and prepared using the Protein Preparation Wizard software. Docking grids of 30 Å × 10 Å were generated around the co-crystallized ligand-binding site. VEG3, a known VEGFR1 inhibitor, was redocked to validate the receptor grid and preserve its native interaction profile. The CRT2 peptide was docked using the ClusPro 2.0 server, and the top ten docked conformations were selected based on the docking energy and structural alignment. Side-chain refinement was applied, and complexes with low binding energies were considered for further analyses. Protein-peptide interactions were visualized and analyzed using PyMOL and LigPlot+. The missing residues (Val990–Leu995) in VEGFR1 were modeled using the PRIME module. Molecular dynamics simulations were conducted using AMBER14 with the ff99SB and GAFF force fields. The systems were neutralized with counter ions and solvated in an 8 Å TIP3P water box. After energy minimization and equilibration, 10 nsec production simulations were performed under NPT conditions (300 K, 1 atm) with a 2 fsec time step. The SHAKE algorithm, Langevin thermostat, and Particle Mesh Ewald method were applied. Snapshots were recorded every 10 psec for each trajectory. The binding free energy was calculated using the MM-PBSA method from the final 100 nsec trajectory data. CPPTRAJ, VMD, and PyMOL were used for structural analysis and visualization.

FITC-conjugation

To construct a fluorescent probe, the N-terminal amino group of the peptide was bound to FITC. The peptides

Box 1: Peptide binding assay

Principle

The assay evaluates the binding affinity of FITC-labeled CRT2 peptide to VEGFR1-expressing HT-116 epithelial cells using flow cytometry and fluorescence microscopy

Requirements

Cells and culture media: HT-116, Dulbecco's Modified Eagle Medium (DMEM), Fetal bovine serum (FBS) – 5%, Phosphate Buffered Saline (PBS) and PBS with 0.05% Tween-20 (PBS-T)

Fixatives and blocking agents: 4% Formaldehyde (for cell fixation), Bovine Serum Albumin (BSA) – 1% Normal goat serum – 10% and glycine – 0.3 M.

Antibodies: Primary antibody against VEGFR1 (mouse monoclonal) and secondary antibody phycoerythrin-labeled anti-mouse IgG.

Procedure

Step 1: To study CRT2's ability to interact with epithelial cells HT-116 (3×10^4 cells/well) treated with FITC-labeled CRT2-peptide (0.35 and 0.75 µM) or FITC labeled src-peptide (0.6 µM) in DMEM media containing 5% fetal bovine serum at 37° C (± 0.5°C) with 5%CO_2 was humidified for 24 hours.

Step 2: Following three PBS washes, the cells were tympanized and reconstituted in PBS for flow cytometry analysis (BD FACS Calibur flow cytometer).

Step 3: HT-116 cells were placed in a 12-well plate and allowed to reach 80% confluence to evaluate CRT2 binding to VEGFR+ cells.

Step 4: After that, in humid conditions, treated for 24 hours using various doses of CRT2 peptide (0.35 and 0.75 µM) and scr peptide (0.6 µM).

Step 5: Following two PBS-Tween (0.05% Tween) washes in each well, tympanized cells were fixed in 4% formaldehyde for 20 min at room temperature.

Step 6: A blocking buffer consisting of 1%BSA, 10% normal goat serum, and 0.3M glycine in 0.1%PBS-T was added after two PBS-Twin washes, and it was left for an hour.

Step 7: The cells were then treated overnight at 4°C with a primary antibody against VEGFR1.

Step 8: After four washes, the anti-mouse IgG secondary antibody was phycoerythrin-labeled and then placed into action.

Step 9: Counterstained cells were examined under a microscope with a fluorescent field.

Reference

Ara et al., 2012

were mixed with a dissolved 1 mg/mL FITC solution in DMSO (Shobeiri et al., 2022). The reactions at pH 8.5 limited the interaction with the arginine and lysine side groups. After that, the tube was covered with foil and placed in an incubator at 37°C for 90 min. The unbound FITC peptides were removed and transferred to the PBS storage buffer. It was placed on a 1.5 x 150 cm sephadex G10 column that had been adjusted and eluted with pH 7.5 PBS (buffer). Then measured at 280 nm phase contrast fluorescent microscope (Nikon TS-100 Olympus, Japan), the concentration of the samples was calculated using the formula:

Peptide (mg/mL) = $(A_{280} \times DF \times MW)/e$,

Where "e" denotes the molar extinction coefficient of each chromophore at 280 nm, DF denotes the dilution factor, and MW stands for peptide molecular weight

MTT assay

HT-116 cell lines (1.0×10^5 cells/well) were treated with CRT2 peptide concentrations (0, 10, and 20 µM) in a 96-well plate. The cultures were incubated for 24 to 48 hours at 37°C ± 0.5°C in a humid environment with 5% CO_2. Administration of 1 mg/mL MTT solution was done for three hours under the same conditions. After incubation, 100 µL of DMSO was added to each well and incubated for another 15 min. The color intensity of MTT formazan was analyzed at 570 to 590 nm using a Multiskan GO microplate multi-spectrophotometer (Thermo Scientific, USA).

AO/EB morphological assay

The AO/EB assay was used to examine both living and dead cells. This experimental protocol is carried out on CRT2 cells treated at IC_{50} concentrations, as well as PBS -treated cells, as the control group. They were incubated with an AO/EB (100 µL/mL) cocktail for 15 min (Wageesha et al., 2017). Cell death was observed under a phase-contrast fluorescent microscope (Nikon TS-100 Olympus, Japan).

Apoptosis and cell cycle assay

HT-116 cells (1.5×10^5 cells) were grown in 6-well plates at 37 ± 0.5°C with 5%CO_2 for 24 hours with IC_{50} concentrations of 0, 10, and 20 µM of CRT2 peptide. To illustrate it briefly, the treated cells were trypsinized and then subjected to a minimum of three ice-cold DPBS washes. Cells were resuspended in 100 µL of DNA binding buffer for 5 min and then stained with 5 µL of annexin V and 10 µL of PI for 10 min at ambient temperature (25°C) (Ahmed, 2020; Fantoukh et al., 2023). The flow cytometry data were analyzed using a Cyto-FLEX flow cytometer (Beckman Cutler Inc., USA).

Weston-blot analysis

Total protein was isolated from the treated HT-116 cell lines using a RIPA buffer cocktail. Roughly 1 mg of the sample was chopped and stored at 4°C for 30 min with a protease cocktail. The mixture was centrifuged at 20,000 x g for 10 min (Han et al., 2019). Total protein

concentration was measured using the Bradford method, NanoDrop (Molecular Devices, USA). In each sample, 20 µg of total protein was used for SDS-PAGE gel running. After being placed into a nitrocellulose membrane, proteins were blocked with 3% bovine serum albumin (BSA) in TBST buffer for 90 min. Primary antibodies against Bax (1:1000), Bcl-2 (1:1000), p-ERK1 (1:1000), p-Akt (1:1000), and VEGF-1 (1:1000) were incubated with blocked membranes and β-actin (1:000). The reference protein was incubated overnight at 4°C. On day two, the membrane was rinsed three times at 10-min intervals using TBST washing buffer. Subsequently, the membrane was treated with goat anti -rabbit conjugated IgG-HRP (1:2000) as the secondary antibody for three hours at room temperature. The blot was rinsed three times with TBST after incubating with the secondary antibody, with a 10-min break between each wash. After washing with TBS-T, the membrane was coated with 1 mL of Pierce ECL western blot substrate (Cat No. 32106). The Gel Dock system, G: Box (Syngene, USA), was then used to identify the protein bands on the membrane.

Statistical analysis

Data were expressed as mean ± SEM. The results were subjected to one-way ANOVA to analyze the differences between the treatment groups and the control groups. A p-value of <0.05 was considered significant.

Results

Molecular interaction predictions with VEGF-A/ VEGFR1 binding pocket

The results suggested that molecular modeling of CRT2 and VEGFR1 had a more promising relationship. Nonetheless, for the binding of VEGFR1 with CTR2 peptide, the highest-scored superimposed structures were employed. The PDB databank (2XAC) provided the protein structures of VEGFR1 and the co-crystal ligand molecule shown in Figure 1A-B. It was determined that the binding energy between CRT2 and VEGFR1 is -37.05 kcal/mol, demonstrating that CRT2 can bind to the VEGFR1 receptor. Moreover, a thorough examination of ligand-protein interactions using Pymol and LigPlot+ revealed that CRT2 interacts with VEGF-B/ VEGFR1 residues, including Glu59, His145, Gln146, Ser186, Trp226, Arg225, and Lys265 through hydrophobic and van der Waals contacts (Figure 1B). The most hydrophobic peptide amino acid residues of CRT2 are found in the van der Waals interaction, specifically Arg4, Ser9, Tyr10, and Met19. The present derivative CRT2: VEGFR1 with all interacting active residues and the full crystal structure of VEGFB: VEGFR1 (PDB ID: 2XAC) are briefly compared according to the VEGFR1 ribbon and surface filling model. CRT2 (stick shape) firmly fits into the kinase pocket (Figure 1C).

Molecular dynamic modeling of CRT2/VEGFR1 interaction under physiological conditions

Under physiological conditions, the stability of the VEGFR1-CRT2 interactions had been validated by molecular dynamics simulation and docking experiments. According to hydrogen bond studies, CRT2 was mostly supported by polar contacts with water molecules and forms hydrogen bonds principally with Glu-59, with a high occupancy value. The molecular docking, CRT2, was able to fit into the VEGFR1 kinase domain pocket with the assistance of seven front and five rear water molecules (Figure 2A (i and ii)). Using all of the default settings from Amber's MMPBSA module, the binding free energies of CRT2 were calculated over the previous 2 nsec simulation frames using the Molecular Mechanics Poisson-Boltzmann Surface

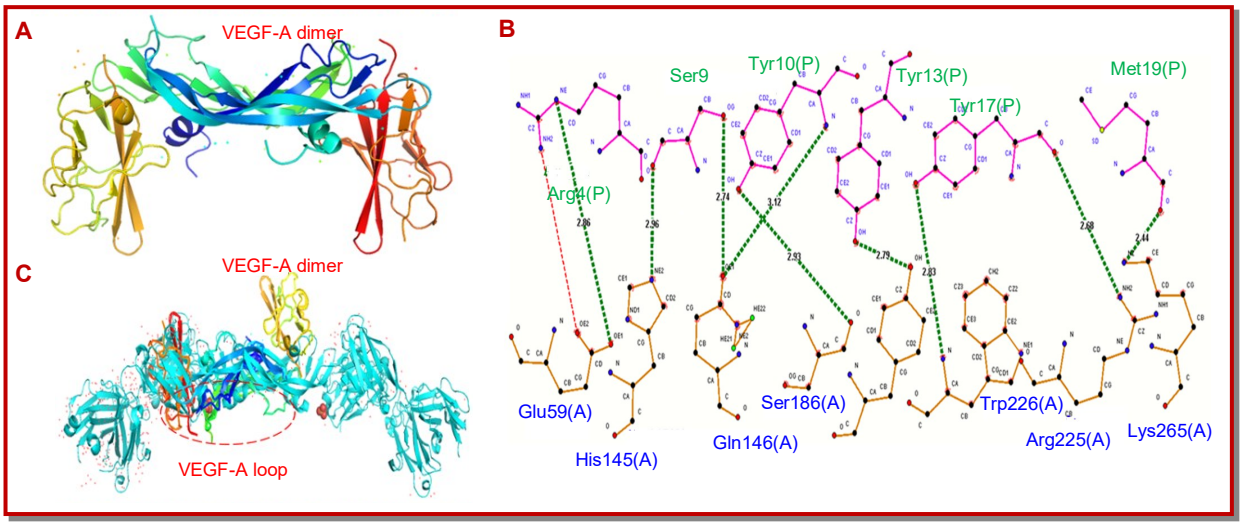

Figure 1: The VEGFR1 protein interacts structurally with CRT2. VEGF-A and VEGFR1 interact (A). The VEGF-A dimer's complex structure with VEGFR1-D1-D6 (B). The CRT2 peptide binds to an overall amino acid in the VEGFR1 site (C). Pymol and LigPlot+ were used to visualise the docking complex. Various ligands that contain CRT2, denoted by green or red hues respectively

Area (MMPBSA) technique (Figure 2B). These findings imply that the electrostatic and van der Waals interactions contribute to the energetically favorable conformational stability of VEGFR1-CRT2. All-atom molecular dynamics simulation research was done on the docked complex to obtain more mechanistic in-sights into the binding behavior of CRT2 with VEGFR1.

We investigated the simulated trajectory in more detail. The system's flexibility and stability were ascertained using B-factor analysis and root mean square displacement (RMSD), as illustrated in Figure 2C. The backbone RMSD of the unbound VEGFR2 and VEGFR2-andrographolide complex was very low (~1.5–2 Å), suggesting that the system remains stable during the simulation and the overall structure did not change signify-cantly from the initial conformation. According to B-factor analysis, when CRT2 bound to the structure, its overall flexibility decreased (Figure 2D).

Interaction assessment in VEGFR1

HT-116 cells were exposed to multiple doses of either FITC-conjugated scr-peptide (0.6 µM) or fluorescein isothiocyanate (FITC)-conjugated CRT2 (0.35 and 0.75 µM) to assess the CRT2 peptide's ability for cell-surface binding. In contrast to the control HT-116 cells and scr-peptide, as demonstrated in Figure 3A. The fluorescence intensity rose greatly as the concentration of FITC -CRT2 increased. To determine if CRT2 binding was due to VEGF receptors, HT-116 cells were treated with anti-VEGFR1 primary antibody, phycoerythrin (PE)-labeled as antibody and FITC-labeled as rabbit anti-mouse IgG secondary antibody that increases the concentration in CRT2 (0.33, 0.75 µM), or scr (0.6 µM). As demonstrated in (Figure 3B), incubation with CRT2 led to a considerable dose-dependent reduction in fluorescence signals when compared to the control and scr peptide (0.6 µM). This result shows that the CRT2 can bind to VEGFR1 on the surface of epithelial cells and compete with antibodies that recognize the extra-cellular domains of the receptors. It was verified by fluorescence microscopy that CRT2 was able to adhere to VEGFR1 on the surface of epithelial cells. HT-116 cells were treated with CRT2 at different doses (0.35 and 0.75 µM), and then PE-labeled goat anti-mouse IgG secondary antibodies and anti-VEGFR1 primary antibodies were added. Fluorescence intensity was lowered by CRT2 in a dose-dependent manner. Only 8% reduction at 0.75 µM concentration, while 78% in the control. This result validates the CRT2's ability to recognize VEGFR1. To confirm further CRT2's VEGFR1 binding characteristics, it is demonstrated in that the highly expressed VEGFR1 colorectal cancer HT-116 cell lines have suppressed their growth.

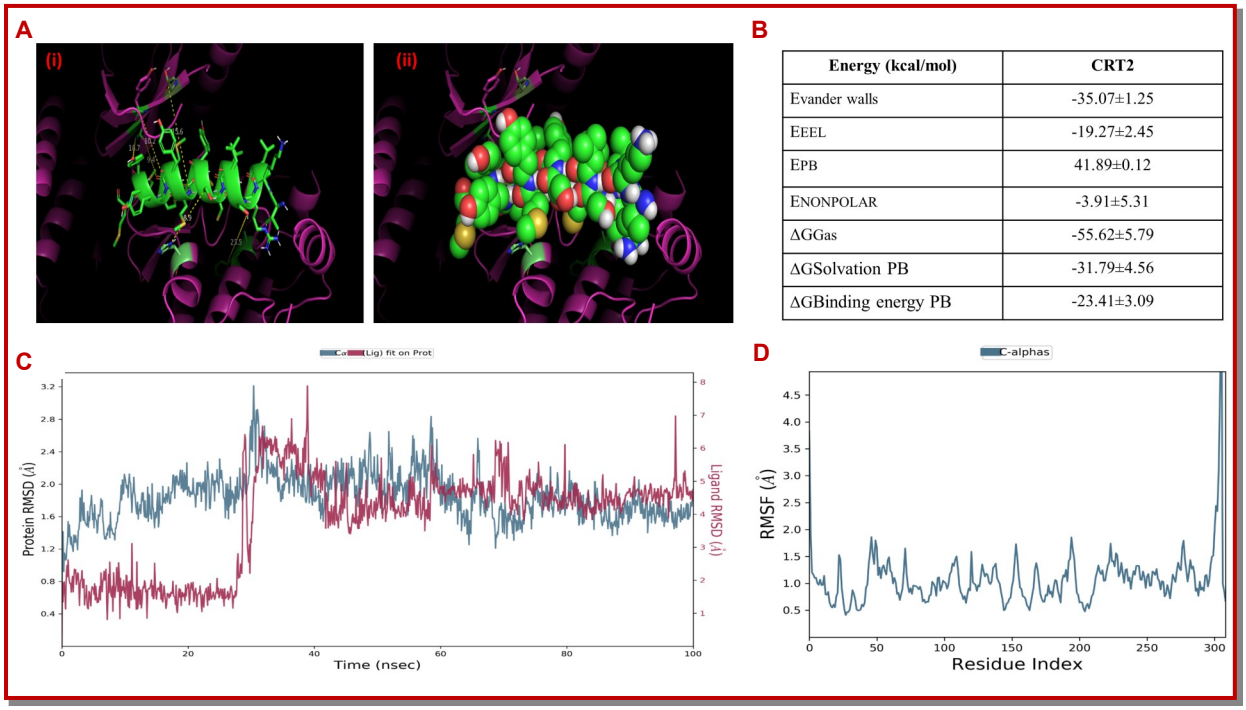

Energy (kcal/mol)	CRT2
Evander walls	-35.07±1.25
EEEL	-19.27±2.45
EPB	41.89±0.12
ENONPOLAR	-3.91±5.31
ΔGGas	-55.62±5.79
ΔGSolvation PB	-31.79±4.56
ΔGBinding energy PB	-23.41±3.09

Figure 2: The docked conformation indicates that the water-mediated interactions are supporting CRT2 binding (A). Using VEGFR1 to bind the free energy component of CRT2 according to MMPBSA calculations (B). The CRT2-VEGFR1 complex and the protein VEGFR1's root mean square displacement (RMSD) (C). B-factor analysis indicates that the upon contact with CRT2, protein flexibility declines (D).

The abbreviations are Evander walls: Non-bonded van der Waals energy; EEEL: Non-bonded electrostatic energy; EPB: Energy of polar solvation (PB); ENPOLAR: Repulsive solute-solvent interactions (PB) that produce nonpolar solvation energy; ΔGGas: Internal energy + EEEL+ EVDWAALS; ΔGsolv: Polar solvation energy plus non-polar solvation energy equals; ΔGGas+ΔGsolv: Binding free energy is binding energy

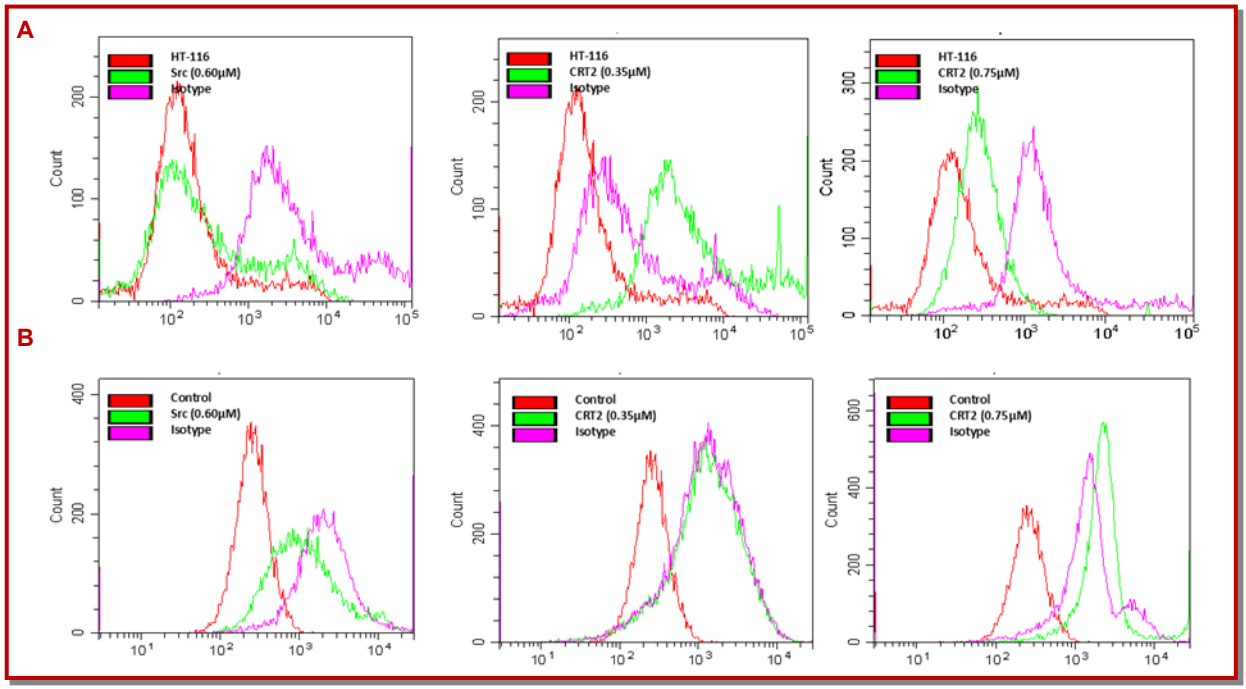

Figure 3: HT-116 cells were coupled with either FITC-scr peptide (0.60 µM) or FITC-CRT2 peptide (0.35 and 0.75 µM) for a predefined amount of time (green curve). The auto fluorescence of the cells is represented by a pink curve (A). HT-116 was exposed to different concentrations of scr peptide (0.60 µM) or CRT2 peptide (0.35 and 0.75 µM) for an entire night in the dark (green curve) (B)

Cell proliferation, morphological changes, and cell invasion

We chose the *in vitro* cell model to study the cytotoxic effects of CRT2 on colorectal cancer VEGFR1+ HT-116 cell lines. These were exposed to varying doses of CRT2 for 24 to 48 hours. CRT2 effectively stopped the proliferation of colorectal cancer cell lines (Figure 4A-B). The half-maximum inhibitory concentration (IC_{50}) of CRT2 for HT-116 cells was 16.0 ± 1.3 µg/mL, respectively. The CRT2 peptide demonstrated a broad spectrum of cell inhibition in a dose- or time-dependent manner in several colorectal cancer cell lines. The peptide contains six positively charged residues that make up a CRT2 peptide, which is soluble in water. One side of the helix, methionine (W), is hydrophobic, and the other side of the helix, h, is polar and hydrophilic amino acids. This is where the CRT2 peptide is located. It is known that these cationic amphipathic peptides can cause membrane instability and cause cancer cells to die. It had been discovered that peptides containing serine caused cell cycle arrest and apoptosis. Phase-contrast microscopy was used to analyze the morphology of selective CRT2 in human colon cancer cell lines. Green light was emitted by living, viable cells, orange-yellow light was emitted by early apoptotic cells, and red light was emitted by late apoptosis or DNA-fragmented cells (Figure 4C). CRT2-treated colorectal cancer cells exhibited an increase in HT-116 apoptosis. Data were synchronized with the MTT.

Mitochondrial potential against CRT2-treated colon cancer cell lines

Anti-cancer properties of CRT2 peptide were further validated by this assay. The regulation of apoptosis was largely dependent on the cell apoptosis. JC-1, a monomer that exhibits green fluorescence at Em485 and Ex535 nm, was used in the MMP-sensitive fluorescent assay to evaluate MMP in the context of CRT2 therapy. In cells with greater mitochondrial potential, JC-1 fluorochrome accumulated within the mitochondrial membrane matrix to form JC-1 fluorochrome aggregation. It exhibited red fluorescence with values of Ex560 and Em595 nm (Figure 5). Due to monomer aggregates in the mitochondria, in this situation, which has low mitochondrial membrane potential, apoptotic cells or JC-1 fluorochrome continue to develop. Consequently, there is a red shift to a green shift in the fluorescence spectrum extension, a measure of mitochondrial depolarization. In both control and free drug-treated cells, the mitochondria displayed red fluorescence. This progression indicated active mitochondria. However, CRT2 treatment reduced mitochondrial integrity in a dose-dependent manner. In contrast to the control group, where CRT2-induced membrane depolarization resulted in loss of mitochondrial integrity, CRT2 therapy enhanced the accumulation of JC-1 monomer in cells. The image clearly illustrates the ratio of red to green fluorescence intensity, cell death, or damage in comparison to control clustered cells. When compared

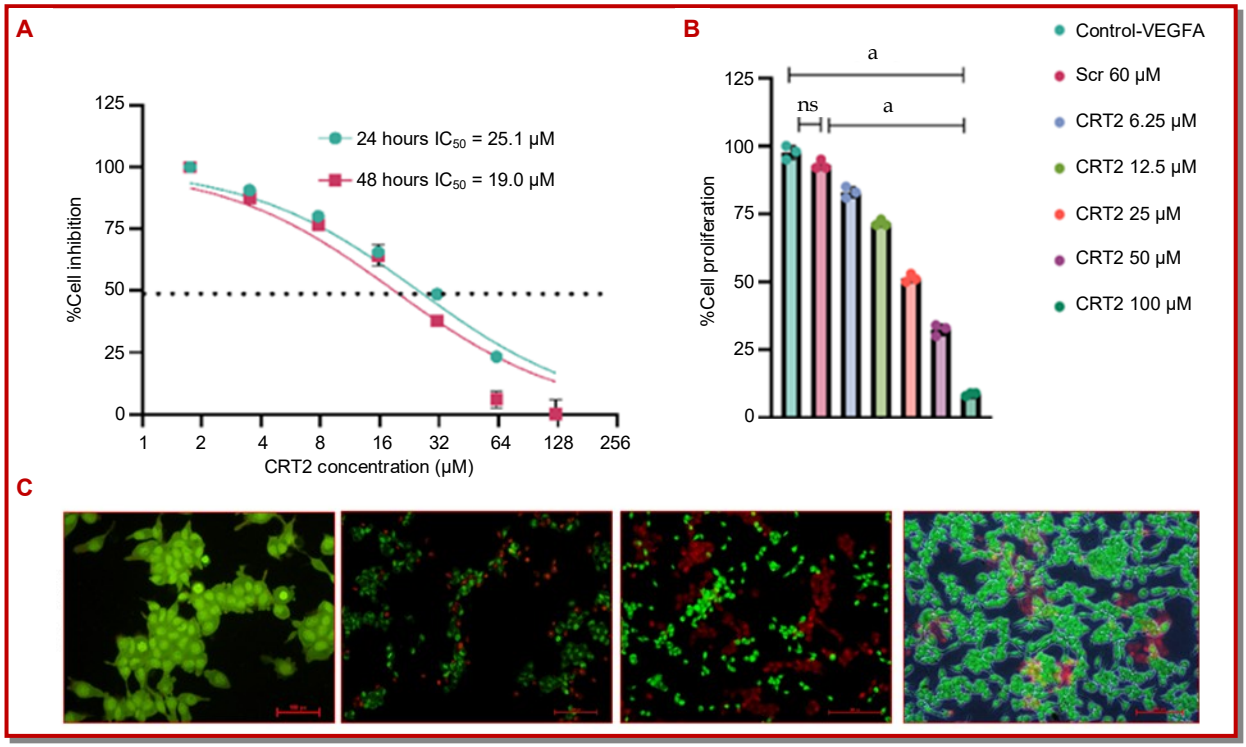

Figure 4: Effects of CRT2 peptide cytotoxicity on HT-116 cancer cells treated for 24 to 48 hours (A and B). Morphological analyses employing HT-116 cell lines treated with CRT2 peptide to distinguish between living, apoptotic, and necrotic cells using the AO/EB staining techniques green and red fluorescence (C) . Data were mean ± SD; n=3. In relation to the control, [a]$p<0.001$

to control cells, CRT2 at 0, 10, and 20 µM displayed a 1.3 -fold drop in mitochondrial membrane potential.

Colony formation of spheroid HT-116 cancer cell lines

In HT-116 cells, CRT2 significantly reduced colony formation as compared to the vehicle (DMSO) group. Phase contrast microscopy was used to show the colony population density in each plate after treatment (Figure 6A). Density measurements compared the control and treatment groups. Colony development was reduced by more than 50% when the CRT2 peptide was administered at 0, 10, and 20 µM, or about half the IC_{50} dose. Moreover, the HT-116 cell line had anti-angiogenic properties. Using the Matrigel invasion assay, the CRT2 therapy of HT-116 cells was evaluated. CRT2 dramatically decreases the invasive capacity of HT-116 cells in a concentration- or dose-dependent manner (Figure 6B).

Apoptosis via the mitochondrial pathway

The apoptotic potential of CRT2 in HT-116 cells was assessed using propidium iodide and annexin V-FITC dual labeling in a flow cytometry study (Figure 7A). After being exposed to their respective IC_{50} values, the HT-116 cell lines increased the fraction of late-apoptotic cells, a total apoptosis rate of 87.3% (Figure 7B). Notably, the number of late apoptotic cells increased significantly. The level of pro- and anti-apoptotic proteins was assessed in both cancer cell lines. CRT2 resulted in a dose-dependent reduction in the levels of anti-apoptotic Bcl-2 despite a considerable increase in the Bax protein level (Figure 7C).

Cell cycle in colorectal cancer cell lines

To ascertain whether a particular cell cycle arrest mediated by the antiproliferative impact of CRT2 on HT-116 cell lines, we examined the cell cycle phase distribution after CRT2 treatment (Figure 8A). CRT2 cells treated with 0, 10, and 20 µM for 24 hours demonstrated a clear cell accumulation during the G1/S phase (Figure 8B). G1/S phase arrest was further confirmed by expression of Cdk, CKIs, and cyclins. In HT-116 cells, CRT2 significantly reduced the amount of cyclin D1 and elevated the expression of the cell cycle inhibitory protein p21 (Figure 8C). The peptide inhibits cell development in HT-116 cancer cells by blocking the cell cycle transition from G1 to S, as observed G1/S phase arrest with CRT2 treatment.

Constitutive and VEGFA-induced phosphorylation of VEGFR1

Like VEGF overexpression, incorrect VEGFR1 activation had been reported in cancer cells, including colorectal cancer cell lines. Dysregulation of downstream signaling is the outcome of VEGFR1 dimerization, which is triggered by phosphorylation that is dependent on the VEGFA ligand. This study investigated the effects of CRT2 in control groups, 10-20 µm over 24 hours on the VEGFR1-positive colorectal cancer cells.

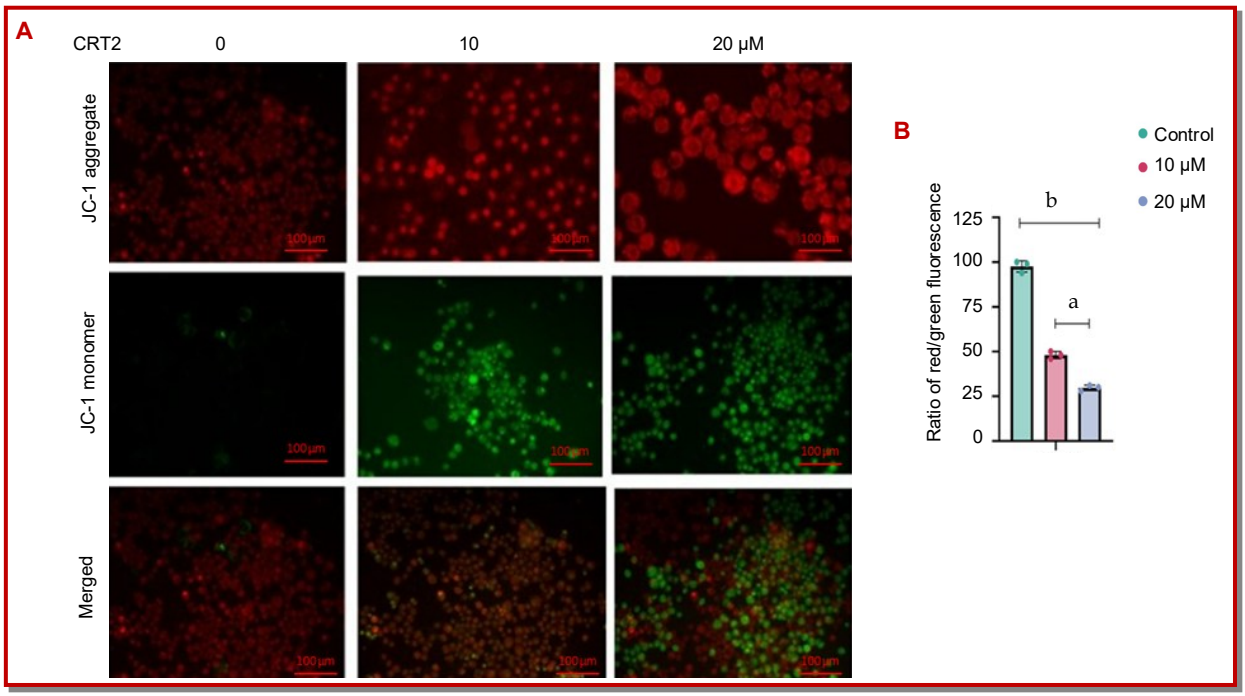

Figure 5: Mitochondrial membrane potential measured in the HT-116 cell lines at 10 and 20 µg/mL (JC-1 monomer aggregates are displayed in green and red), with a scale bar of 100 µm. The measurement of the red to green relative fluorescence of JC-1 for control, HT-116 cells treated with 10 and 20 µm. the data were expressed as SEM (n=3), [a]p<0.05 and [b]p<0.0001; Magnification 40x

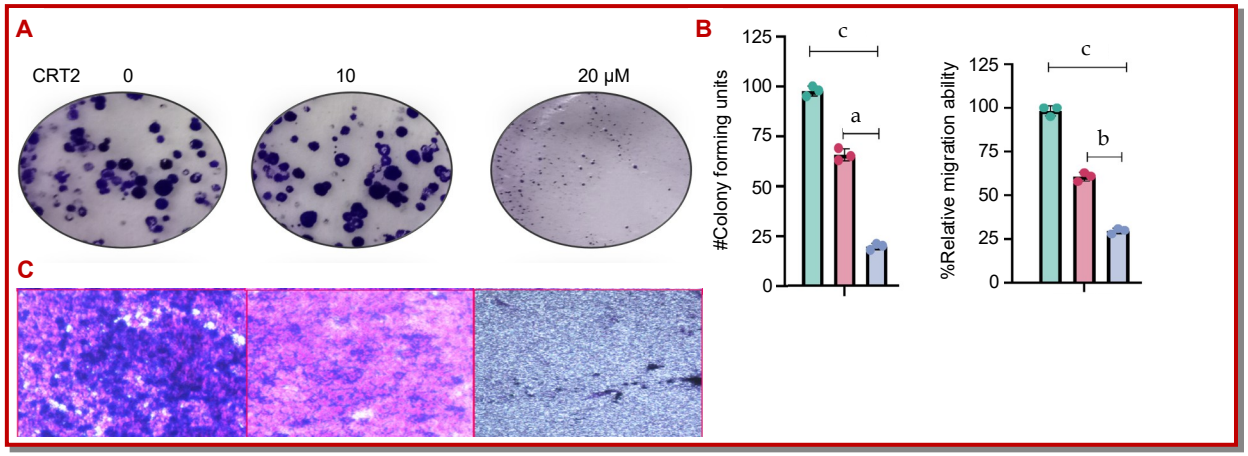

Figure 6: After pre-treating HT-116 cell lines with CRT2 peptide for 24 hours, the cells were plated at a density of 500 cells per well for 15 days to create colony forming pictures. Following the colonies' fixation and 0.5% crystal violet staining (A). Assay for Transwell invasion CRT2 0, 10, and 20 µg/mL were used to seed HT-116 cells in the upper chamber over a 24-hours period. Preserved, labelled, and counted the migrating cells in the lower chamber and images from three separate tests (B-C). With respect to the control group, data were mean ± SEM; n=5; [a]p<0.05, [b]p<0.01, and [c]p<0.0001; Magnification 40x

This subsequently started mitogenic, chemotactic, and pro-survival signals, as well as tumor vascular growth. The VEGFR1 expression was significantly reduced by CRT2 treatment at concentrations of 10 and 20 µM. CRT2 decreased the fold changes in activation phosphorylation protein via VEGFR1. The protein fold changes 1.2 and 1.5 compared to the control groups vs CRT treatments. These results unequivocally show that the constitutive VEGFA-induced activation is suppressed by CRT2 treatment. Moreover, VEGFA/VEGFR1 phosphorylates several downstream substrates of PI3K/Akt signaling which is implicated in important physiological processes such as cell division and cell death. In HT-116 cells, CRT2 treatment decreased the expression of PI3K's regulatory subunit p85 and a catalytic subunit, p110. By suppressing the functions of pro-apoptotic proteins and promoting the expression of cell-survival proteins, PI3K regulates the phosphorylation and activation of Akt, which enhances cell survival. Due to CRT2's PI3K inhibition, Akt phosphorylation

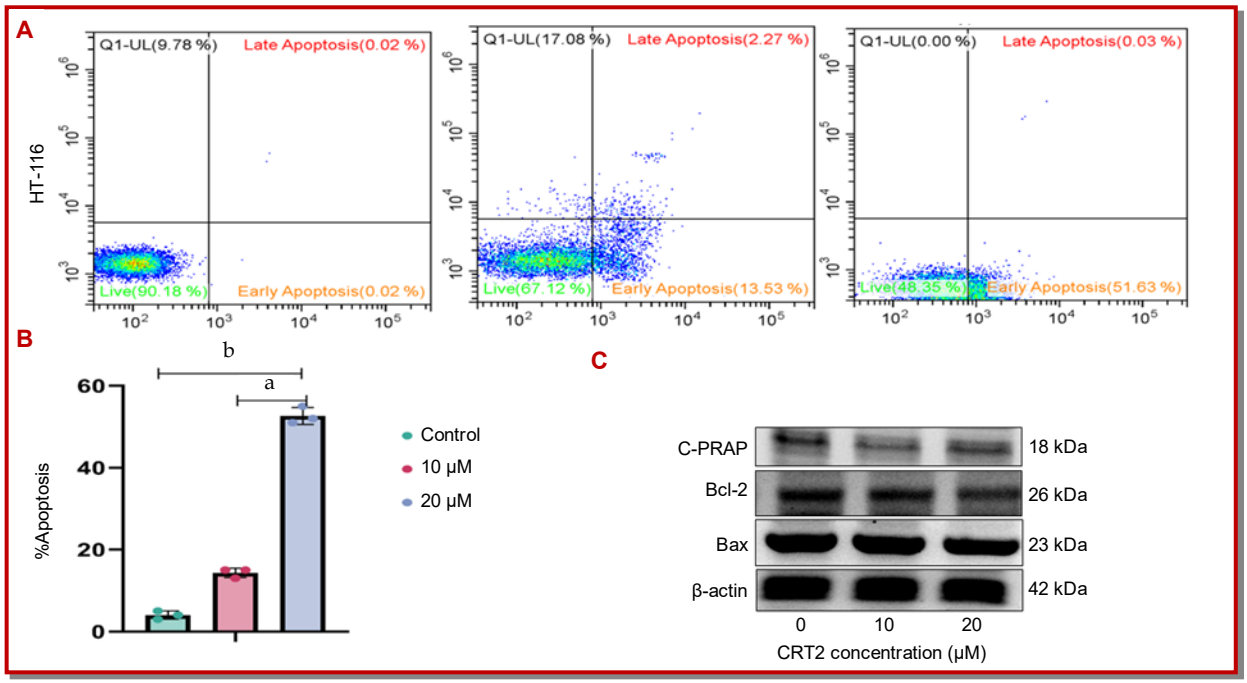

Figure 7: Effects of CRT2 on apoptosis (A-B) and proteins Bax/Bcl-2 (C) of HT-116 cells. With respect to the control group, data were expressed as mean ± SEM; n=5; [a]p<0.05; [b]p<0.01

significantly dropped in HT-116 cells (Figure 9A). The MAPK pathway is another signaling cascade that is triggered by VEGFR and is essential for regulating several physiological reactions, including cell division and cell death. The three main subgroups of the MAPK family are p38 MAPK, c-Jun N-terminal kinase (JNK), and extracellular signal-regulated protein kinase (ERK). While JNK and p38 MAPKs are involved in apoptotic cell death, ERKs are involved in the regulation of mitogen-activated proliferation/differentiation factors (Figure 9B). The CRT2 therapy significantly reduced p38, JNK1/2, and ERK1/2 phosphorylation in HT-116 cells by 1.2 to 1.5-fold reduction.

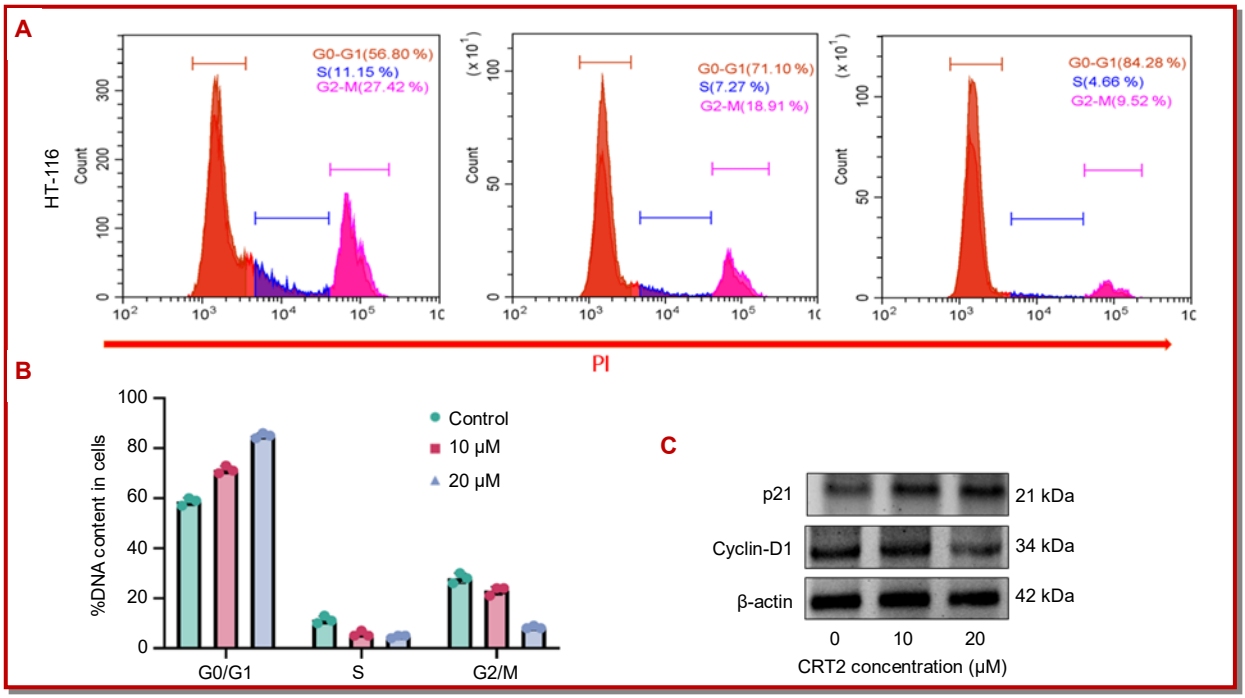

Figure 8: Effects of CRT2 on cell cycle analysis using flow cytometry analysis (A), DNA content (B), and cyclin-D/p21 proteins (C) in HT-116 cells. Data were mean ± SEM; n=5

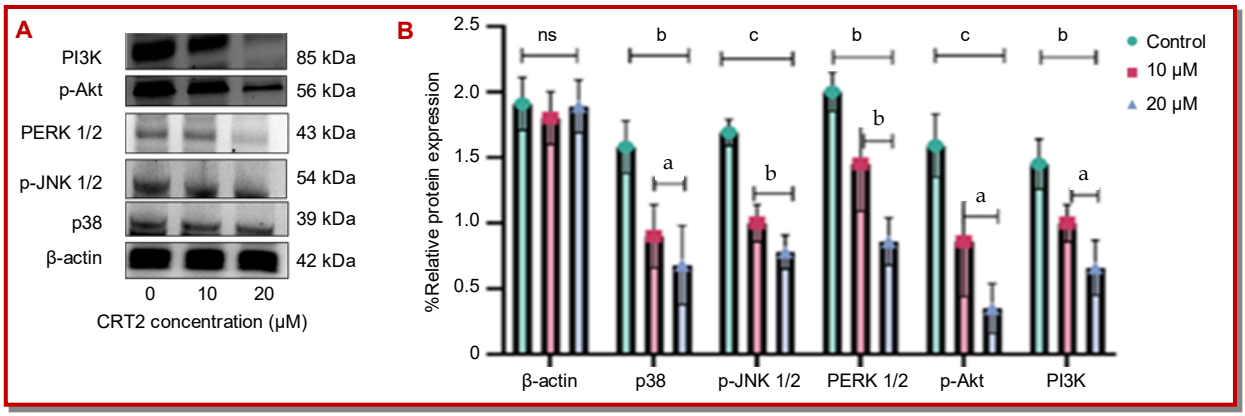

Figure 9: Western blot analysis showing the effect of CRT2 on the expression of p-MEK, p-ERK1/2, and p-Akt in HT-116 colorectal cancer cells (A). Densitometric quantification of p-MEK, p-ERK1/2, and p-Akt levels normalized to β-actin (B). Data were presented as mean ± SEM; n=5; $^{a}p<0.05$; $^{b}p<0.01$; $^{c}p<0.0001$ vs. control

Discussion

In the current study, the CRT2 peptide was successfully synthesized, exhibiting a molecular weight of 2,228.8kDa and a purity of ≥95%. The peptide contains six positively charged residues and is hydrophilic. Structurally, one side of the α-helix is composed of methionine residues, making it hydrophobic, while the opposite side consists of polar and hydrophilic amino acids. This amphipathic configuration characterizes the CRT2 peptide. As a cationic amphipathic peptide, CRT2 can induce membrane instability, leading to cell proliferation and cell death.

Molecular docking analysis revealed a strong binding affinity between CRT2 and VEGFR1, with a minimum binding energy of –37.05 kcal/mol. This binding interaction was visualized through structural superimposition, which showed that CRT2 interacts with several key residues in the VEGF-B/VEGFR1 complex, including Glu59, His145, Gln146, Ser186, Trp226, Arg225, and Lys265. These interactions involve both hydrophobic and van der Waals forces. Notably, the most hydrophobic amino acid residues of CRT2—Arg4, Ser9, Tyr10, and Mept19 participated in van der Waals interactions, contributing to the peptide's strong binding and potential anti-cancer activity. Similarly, *in vitro* studies revealed that CRT2 binds to VEGFR1 on the surface of epithelial cells and competes with antibodies that recognize the extracellular domains of the receptors. Based on the MMT assay, the results of CRT2 treatment in HT-116 cells were 16.0 ± 1.3 μg/mL, respectively. Annexin V-FITC (fluorescein isothiocyanate) and propidium iodide double labeling after CRT2 treatment confirmed its ability to induce apoptosis and cell cycle arrest. Apoptosis is down-regulated when VEGFR, PI3K/Akt, or MAPK are activated; therefore, one of the most obvious targets for cancer therapy is apoptosis activation (Tokunaga et al., 2008). Anti-apoptotic (Bax and Bak) and pro-apoptotic (Bcl2, Bcl-xL, and Mcl-1) proteins make up the Bcl2 family of proteins, which are significant apoptotic regulators (Mc Cubrey et al., 2006). When CRT2 was applied to colorectal cancer cell lines, the anti-apoptotic protein Bcl2 was found to be less expressed, whereas the pro-apoptotic protein Bax was more expressed.

Caspases are cellular substrates that include the cytoplasm and nucleus, which are essential for structural elements as well as elements of the DNA repair mechanism, such as protein kinase and PARP (Pravdic, 2023; Cingeetham et al., 2015). In the present study, CRT2 therapy induced significant caspase-3 activation and simultaneous PARP cleavage in CRC cells. These MAPKs mediate cell survival and proliferation by phosphorylating various cellular substrates. Moreover, CRT2 therapy increased the expression of p21 and decreased that of cyclin D1, both of which are necessary for cell proliferation. G1/S phase cell cycle arrest was inhibited by CRT2 treatment. In addition, vascular endothelial growth factor receptor-1 (VEGFR1) interacts with its ligands, VEGF-A or VEGF-B, to activate cellular phenotypic modification associated with tumor progression and invasion (Jin et al., 2020). The activation of downstream signaling pathways of JNK/1, ERK-1/2, and MAPK primes cell proliferation, migration, and metastasis. Current CRT2 treatments significantly affect JNK1/2 and ERK1/2 phosphorylation protein expression in CRC cells by 1.21 and 1.5 folds. These findings suggest CRT2 inhibits VEGFR1-persuaded activations.

A study shows that a peptide isolated from garlic (VS9) exhibited an anti-cancer effect against leukemic and HT-116 cell lines via interaction with Bcl-2 family proteins (Rasaratnam et al., 2021). Here, this study first evaluates the effects of CRT2 on the identity compound, which exhibited specific cytotoxic activity in HT-116 cells, and initiated cell apoptosis and cell cycle arrest in a dose- and time-dependent manner. Second, CRT2 inhibited the protein expression of PI3K and Akt at the post-translational levels and reduced the levels of ERK/1 and JNK1. Finally, CRT2 was inhibited by VEGFR1

kinase-induced cell proliferation via PI3K/Akt/ERK1/JNK signal transduction in HT-116 cells.

A primary limitation of the present study is its reliance on *in silico* molecular docking and *in vitro* assays using colorectal cancer cell lines (HT-116). While these approaches provide valuable preliminary insights, the absence of *in vivo* animal model experiments limits the ability to evaluate the systemic efficacy, bioavailability, pharmacokinetics, and potential toxicity of CRT2 under physiological conditions.

Conclusion

CRT-2 peptide constructs targeting the VEGFA/VEGFR1-binding region inhibited proliferation and angiogenesis in VEGFR1-positive HCT-116 cells by suppressing VEGFR1, PI3K, and ERK1/2 signaling. Apoptosis was enhanced via p58 upregulation and Bcl-2 downregulation, indicating CRT2's potential as a promising therapeutic agent for cancer treatment.

Financial Support

Self-funded

Ethical Issue

The guidelines about the development, acquisition, authentication, cryopreservation, and transfer of cell lines between laboratories were strictly followed. Besides, microbial contamination (commonly mycoplasma), characterization, instability, and misidentification was considered seriously.

Conflict of Interest

Authors declare no conflict of interest

Acknowledgement

Authors would like to thank P. S. G. Son's and Charity and Tamil Nadu Dr. M. G. R. Medical University Chennai for providing us with a better facility and environment to this study

References

Ahmed AG, Hussein UK, Ahmed AE, Kim KM, Mahmoud HM, Hammouda O. Mustard seed (*Brassica nigra)* extract exhibits antiproliferative effect against human lung cancer cells through differential regulation of apoptosis, cell cycle, migration, and invasion. Molecules 2020; 25: 2069.

Ara Mst N, Hyodo M, Ohga N, Hida K, Harashima H. Development of a novel DNA aptamer ligand targeting to primary cultured tumor endothelial cells by a cell-based SELEX method. PLoS ONE. 2012; 7: 50-74.

Baidoun, F, Elshiwy K, Elkeraie Y, Merjaneh Z, Khoudari G, Sarmini, M T, Gad M, Al-Husseini M, Saad A. Colorectal cancer epidemiology: Recent trends and impact on outcomes. Curr Drug Targets. 2021; 22: 998-1009.

Behelgardi M, Zahri S, Mashayekhi F, Mansouri K, Asghari SM. A peptide mimicking the binding sites of VEGF-A and VEGF-B inhibits VEGFR-1/-2 driven angiogenesis, tumor growth and metastasis. Sci Rep. 2018; 8: 17-24.

Cingeetham A, Vuree S, Dunna NR, Gorre M, Nanchari SR, Edathara PM. Influence of BCL2-938 and BAX-248 promoter polymorphisms in the development of AML: Case-control study from South India. Tumor Biol. 2015; 36: 7967-76.

Dey D K, Kang S C. CopA3 peptide induces permanent cell-cycle arrest in colorectal cancer cells. Mechanisms of ageing and development. 2021; 11: 14-27.

Dia VP, Krishnan HB. BG-4 a novel anticancer peptide from bitter gourd *Momordica charantia* promotes apoptosis in human colon cancer cells. Sci Rep. 2016; 1: 165-84.

Fantoukh OI, Al-Hamoud GA, Nasr FA, Almarfadi OM, Hawwal MF, Ali Z. Revisiting the flora of Saudi Arabia phytochemical and biological investigation of the endangered plant species Euphorbia Saudi Arabica. J Metabolites. 2023; 13: 55-62.

Han KY, Chang JH, Azar DT. MMP14 containing exosomes cleave VEGFR1 and promote VEGFA-induced migration and proliferation of vascular endothelial cells. Invest Ophthalmol Visual Sci. 2019; 60: 23-31.

He L, Lu N, Dai Q, Zhao Y, Zhao L, Wang, H Li Z, You Q, Guo Q. Wogonin induced G1 cell cycle arrest by regulating Wnt/β-catenin signaling pathway and inactivating CDK8 in human colorectal cancer carcinoma cells. Toxicology 2013; 31: 36-47.

Jin C, Chen J, Cheng Y, Fu Y, Zhao H, Tang M. Mesenchymal stem cell-derived exosomes protect beta cells against hypoxia-induced apoptosis via miR-21 by alleviating ER stress and inhibiting p38 MAPK phosphorylation. Curr Cancer Drug Targ. 2020; 11: 65-79.

Mabeta P, Steenkamp V. The VEGF/VEGFR axis revisited implications for cancer therapy. Int J Mol Sci. 2022; 24: 155-85.

Mc Cubrey JA, Steelman LS, Abrams SL, Lee JT, Chang F, Bertrand FE. Roles of the RAF/MEK/ERK and PI3K/PTEN/Akt pathways in malignant transformation and drug resistance. Adv Enzyme Reg. 2006; 46: 249-79.

McCauley J, Zivanovic A, Skropeta D. Bioassays for anticancer activities. Methods Mol Biol. 2013; 55: 191-205.

Pravdic Z, Vukovic NS, Gasic V, Marjanovic I, Karan-Djurasevic T, Pavlovic S. The influence of BCL2 BAX and ABCB1 gene expression on prognosis of adult *de novo* acute myeloid leukemia with normal karyotype patients. Radiol Oncol. 2023; 57: 239-48.

Rasaratnam K, Nantasenamat C, Phaonakrop N, Roytrakul S, Tanyong D. A novel peptide isolated from garlic shows anticancer effect against leukemic cell lines via interaction with Bcl-2 family proteins. Chem Biol Drug Des. 2021; 97: 17-28.

Santhosha SG, Jamuna P, Prabhavathi SN. Bioactive compo-

nents of garlic and their physiological role in health maintenance. Food Biosci. 2013; 3: 59-74.

Shobeiri SS, Sankian M. Polyvinyl alcohol can stabilize FITC conjugated recombinant annexin V for apoptotic cells detection. Protein Pep Lett. 2022; 29: 806-14.

Tokunaga E, Oki E, Egashira A, Sadanaga N, Morita M, Kakeji Y. Deregulation of the Akt pathway in human cancer. Curr Cancer Drug Targ. 2008; 8: 27-36.

Wageesha ND, Soysa P, Atthanayake K, Choudhary MI, Ekanayake M. A traditional poly herbal medicine "Le Pana Guliya" induces apoptosis in HepG 2 and HeLa cells but not in CC1 cells: An *in vitro* assessment. Chem Central J. 2017; 2017.

Wang R, Ma Y, Zhan S, Zhang G, Cao L, Zhang X, Shi T, Chen W. B7-H3 promotes colorectal cancer angiogenesis through activating the NF-κB pathway to induce VEGFA expression. Cell Death Dis. 2020; 11: 55-68.

Weitz J, Koch M, Debus J, Hohler T, Galle PR, Buchler MW. Colorectal cancer. Lancet 2005; 90: 153-65.

Yogananthan D, Raj A., Venkatachalam K, Muthaiah R. A selectivity of super-short peptide morphed hydrophilic and hydrophobic domains to improve anti-cancer efficacy. Eur Chem B. 2023; 12: 5381-88.

Zanjanchi P, Asghari SM, Mohabatkar H, Shourian M, Shafiee Ardestani M. Conjugation of VEGFR1/R2-targeting peptide with gold nanoparticles to enhance antiangiogenic and antitumoral activity. J Nanobiotechnol. 2022; 20: 7-21.

Zhang D, Li X, Song D, Chen S, Zhang Z, Cao S, Liu M. Atractylenolide III induces apoptosis by regulating the bax/bcl-2 signaling pathway in human colorectal cancer HCT-116 cells *in vitro* and *in vivo*. Anti-cancer Drugs. 2021; 33: 30-47.

Author Info

Ramanathan Muthiah (Principal contact)
e-mail: ramanathanm@psgpharma.ac.in